Advances in Applied Mathematics and Mechanics
Adv. Appl. Math. Mech., Vol. 7, No. 2, pp. 180-195

DOI: 10.4208/aamm.2014.m605
April 2015

A High-Order Numerical Method to Study Three-Dimensional Hydrodynamics in a Natural River

Luyu Shen[1,2], Changgen Lu[1,*], Weiguo Wu[3] and Shifeng Xue[3]

[1] *College of Marine Sciences, Nanjing University of Information Science and Technology, Nanjing 210044, China*
[2] *College of Atmospheric Sciences, Nanjing University of Information Science and Technology, Nanjing 210044, China*
[3] *Department of Engineering Mechanics, China University of Petroleum, Dongying 266555, China*

Received 1 May 2014; Accepted (in revised version) 20 August 2014

Abstract. A high-order numerical method for three-dimensional hydrodynamics is presented. The present method applies high-order compact schemes in space and a Runge-Kutta scheme in time to solve the Reynolds-averaged Navier-Stokes equations with the k-ϵ turbulence model in an orthogonal curvilinear coordinate system. In addition, a two-dimensional equation is derived from the depth-averaged momentum equations to predict the water level. The proposed method is first validated by its application to simulate flow in a 180° curved laboratory flume. It is found that the simulated results agree with measurements and are better than those from SIMPLEC algorithm. Then the method is applied to study three-dimensional hydrodynamics in a natural river, and the simulated results are in accordance with measurements.

AMS subject classifications: 65M06, 76F60, 35Q35

Key words: Compact scheme, three-dimensional hydrodynamics, k-ϵ turbulence model, orthogonal curvilinear coordinate system, Runge-Kutta scheme.

1 Introduction

Numerical simulation of fluid motions in natural rivers, reservoirs, bays or harbors is a challenging issue in computational fluid dynamics (CFD), because of their turbulent nature, multi-scale secondary currents, irregular geometry, etc. To essentially solve this problem, one has to use the three-dimensional hydrodynamic models, since

*Corresponding author.
Email: shenluyu99@foxmail.com (L. Shen), cglu@nuist.edu.cn (C. Lu), mailtowwg@gmail.com (W. Wu), xuesf@126.com (S. Xue)

 ©2015 Global Science Press

https://doi.org/10.4208/aamm.2014.m605 Published online by Cambridge University Press

the one-dimensional and two-dimensional models cannot properly describe the three-dimensional flow features such as secondary currents and three-dimensional turbulence [1]. The use of suitable mathematic models is one of the key issues in the three-dimensional hydrodynamic study. The Reynolds-averaged Navier-Stokes (RANS) equations with the k-ϵ turbulence model have been shown to describe three-dimensional flow adequately in many hydraulic applications. Demuren and Rodi [2] used a modified k-ϵ model to study flow in a meandering channel. Ye and McCorquodale [3] simulated three-dimensional free surface flow with a k-ϵ model taking account into anisotropic effects. Wu et al. [4] simulated flow and sediment transport in a 180° bend with the k-ϵ model. More recent simulations are presented by Rüther and Olsen [5], Zhang and Shen [6] and Khosronejad et al. [7].

In the previous studies, the normally used numerical methods of three-dimensional hydrodynamic models are SIMPLE algorithm and its variants such as SIMPLEC, SIMPLEX, and PISO. Zhang and Shen [6] used SIMPLEC algorithm to investigate the river transport of pollution. Feurich and Olsen [8] used SIMPLE algorithm for computing the water flow in a non-orthogonal, structured grid with a non-staggered variable placement. Zeng et al. [9] used a fractional step method to solve the RANS equations in generalized curvilinear coordinates. The advantage of using SIMPLE algorithm is to keep numerical conservation, and the drawback is difficult to extend the method with high-order accuracy which may not match the growing need of hydrodynamics simulations. To remedy the drawback, we will use high-order compact schemes to do spatial discretization. Compact schemes, which were proposed from a generalization of the classical Padé schemes by Lele [10], are high-order schemes extensively applied in Direct Numerical Simulation (DNS) [11,12] and Large Eddy Simulation (LES) [13,14] for turbulence simulation. In our research, the compact schemes are extended to study three-dimensional hydrodynamics.

In our work, a high-order upwind-biased compact scheme [15] is used for convection term discretization on purpose to suppress the spurious waves. For temporal discretization, a Runge-Kutta time stepping scheme is employed. To apply the uniform mesh-based compact schemes for problems with complex geometry, a coordinate transformation is introduced to transform the governing equations in the physical space into those in the curvilinear coordinate system so that the computational domain is always regular and that a uniform mesh can be used. To predict the water level, a two-dimensional equation is derived from the depth-averaged momentum equation following the work of Wu et al. [4]. The flow in a 180° curved laboratory flume [16] is simulated to evaluate the performance of the new method. Then, the proposed method is applied to study the three-dimensional hydrodynamics in a natural river.

2 Governing equations and boundary conditions for flow field

The three-dimensional hydrodynamic model is composed of the incompressible Reynolds-averaged Navier-Stokes equations and standard k-ϵ turbulence model. The continuity and momentum equations in an orthogonal curvilinear coordinate are written

https://doi.org/10.4208/aamm.2014.m605 Published online by Cambridge University Press

as

$$\frac{\partial uH_2H_3}{\partial\xi}+\frac{\partial vH_1H_2}{\partial\eta}+\frac{\partial wH_1H_2}{\partial\zeta}=0, \tag{2.1a}$$

$$\begin{aligned}&\frac{\partial u}{\partial t}+\frac{u}{H_1}\frac{\partial u}{\partial\xi}+\frac{v}{H_2}\frac{\partial u}{\partial\eta}+\frac{w}{H_3}\frac{\partial u}{\partial\zeta}+\frac{v}{H_1H_2}\Big(u\frac{\partial H_1}{\partial\eta}-v\frac{\partial H_2}{\partial\xi}\Big)+\frac{w}{H_1H_3}\Big(u\frac{\partial H_1}{\partial\zeta}-w\frac{\partial H_1}{\partial\xi}\Big)+\frac{1}{H_1}\frac{\partial p}{\partial\xi}\\&=\frac{1}{H_1H_2H_3}\Big(\frac{\partial\tau_{11}H_2H_3}{\partial\xi}+\frac{\partial\tau_{12}H_1H_3}{\partial\eta}+\frac{\partial\tau_{13}H_1H_2}{\partial\zeta}\Big)+\frac{1}{H_1H_2}\Big(\tau_{12}\frac{\partial H_1}{\partial\eta}-\tau_{22}\frac{\partial H_2}{\partial\xi}\Big)\\&\quad+\frac{1}{H_1H_3}\Big(\tau_{13}\frac{\partial H_1}{\partial\zeta}-\tau_{33}\frac{\partial H_3}{\partial\xi}\Big),\end{aligned} \tag{2.1b}$$

$$\begin{aligned}&\frac{\partial v}{\partial t}+\frac{u}{H_1}\frac{\partial v}{\partial\xi}+\frac{v}{H_2}\frac{\partial v}{\partial\eta}+\frac{w}{H_3}\frac{\partial v}{\partial\zeta}+\frac{w}{H_2H_3}\Big(v\frac{\partial H_2}{\partial\zeta}-w\frac{\partial H_3}{\partial\eta}\Big)+\frac{u}{H_1H_2}\Big(v\frac{\partial H_2}{\partial\xi}-u\frac{\partial H_1}{\partial\eta}\Big)+\frac{1}{H_2}\frac{\partial p}{\partial\eta}\\&=\frac{1}{H_1H_2H_3}\Big(\frac{\partial\tau_{12}H_2H_3}{\partial\xi}+\frac{\partial\tau_{22}H_1H_3}{\partial\eta}+\frac{\partial\tau_{23}H_1H_2}{\partial\zeta}\Big)+\frac{1}{H_1H_2}\Big(\tau_{12}\frac{\partial H_2}{\partial\xi}-\tau_{11}\frac{\partial H_1}{\partial\eta}\Big)\\&\quad+\frac{1}{H_2H_3}\Big(\tau_{23}\frac{\partial H_2}{\partial\zeta}-\tau_{33}\frac{\partial H_3}{\partial\eta}\Big),\end{aligned} \tag{2.1c}$$

$$\begin{aligned}&\frac{\partial w}{\partial t}+\frac{u}{H_1}\frac{\partial w}{\partial\xi}+\frac{v}{H_2}\frac{\partial w}{\partial\eta}+\frac{w}{H_3}\frac{\partial w}{\partial\zeta}+\frac{u}{H_1H_3}\Big(w\frac{\partial H_3}{\partial\xi}-u\frac{\partial H_1}{\partial\zeta}\Big)+\frac{v}{H_2H_3}\Big(w\frac{\partial H_3}{\partial\eta}-v\frac{\partial H_2}{\partial\zeta}\Big)+\frac{1}{H_3}\frac{\partial p}{\partial\zeta}\\&=\frac{1}{H_1H_2H_3}\Big(\frac{\partial\tau_{13}H_2H_3}{\partial\xi}+\frac{\partial\tau_{23}H_1H_3}{\partial\eta}+\frac{\partial\tau_{33}H_1H_2}{\partial\zeta}\Big)+\frac{1}{H_1H_3}\Big(\tau_{13}\frac{\partial H_3}{\partial\xi}-\tau_{11}\frac{\partial H_1}{\partial\zeta}\Big)\\&\quad+\frac{1}{H_2H_3}\Big(\tau_{23}\frac{\partial H_3}{\partial\eta}-\tau_{22}\frac{\partial H_2}{\partial\zeta}\Big),\end{aligned} \tag{2.1d}$$

where u, v and w are the velocity-components in the ξ, η and ζ directions respectively; ξ is the streamwise direction, η is the lateral direction, and ζ is the vertical direction. The gravity force is included in the residual kinetic pressure (divided by density) p, i.e.,

$$p=P+P_0-g(h-z).$$

Here P =the kinetic pressure; P_0 =the free surface kinetic pressure; g =the gravitational acceleration; h =the water level; and $h-z$ =the water depth. The stress τ_{ij} includes the viscous stress and Reynolds stress; H_i $(i=1,2,3)$ are the Lamé coefficients of orthogonal curvilinear coordinate defined as

$$H_i=\sqrt{\sum_{j=1}^{3}\Big(\frac{\partial x_j}{\partial\xi_i}\Big)^2},$$

where ξ_1, ξ_2 and ξ_3 are the coordinate axes ξ, η and ζ in the computational domain; x_1, x_2 and x_3 are the coordinate axes x, y and z in the physical space. The stresses τ_{ij} are given by

$$\tau_{11}=(v+v_t)\frac{2}{H_1}\Big(\frac{\partial u}{\partial\xi}+\frac{v}{H_2}\frac{\partial H_1}{\partial\eta}+\frac{w}{H_3}\frac{\partial H_1}{\partial\zeta}\Big),$$

https://doi.org/10.4208/aamm.2014.m605 Published online by Cambridge University Press

$$\tau_{22}=(v+v_t)\frac{2}{H_2}\Big(\frac{\partial v}{\partial\eta}+\frac{u}{H_1}\frac{\partial H_2}{\partial\xi}+\frac{w}{H_3}\frac{\partial H_2}{\partial\zeta}\Big),$$
$$\tau_{33}=(v+v_t)\frac{2}{H_3}\Big(\frac{\partial w}{\partial\zeta}+\frac{u}{H_1}\frac{\partial H_3}{\partial\xi}+\frac{v}{H_2}\frac{\partial H_3}{\partial\eta}\Big),$$
$$\tau_{12}=(v+v_t)\Big[\frac{1}{H_2}\frac{\partial u}{\partial\eta}+\frac{1}{H_1}\frac{\partial v}{\partial\xi}-\frac{1}{H_1H_2}\Big(u\frac{\partial H_1}{\partial\eta}+v\frac{\partial H_2}{\partial\xi}\Big)\Big],$$
$$\tau_{23}=(v+v_t)\Big[\frac{1}{H_3}\frac{\partial v}{\partial\zeta}+\frac{1}{H_2}\frac{\partial w}{\partial\eta}-\frac{1}{H_2H_3}\Big(v\frac{\partial H_2}{\partial\zeta}+w\frac{\partial H_3}{\partial\eta}\Big)\Big],$$
$$\tau_{13}=(v+v_t)\Big[\frac{1}{H_1}\frac{\partial w}{\partial\xi}+\frac{1}{H_3}\frac{\partial u}{\partial\zeta}-\frac{1}{H_1H_3}\Big(w\frac{\partial H_3}{\partial\xi}+u\frac{\partial H_1}{\partial\zeta}\Big)\Big],$$

where v=the kinematic viscosity; the eddy viscosity v_t is calculated by

$$v_t=\frac{C\mu\cdot k^2}{\epsilon}.$$

The turbulent kinetic energy k and the turbulent dissipation rate ϵ are obtained from k-ϵ equations:

$$\frac{\partial k}{\partial t}+\frac{u_j}{H_j}\frac{\partial k}{\partial\xi_j}=\frac{1}{H_j}\frac{\partial}{\partial\xi_j}\Big(\frac{\Gamma_k}{H_j}\frac{\partial k}{\partial\xi_j}\Big)+P_k-\epsilon, \tag{2.2a}$$
$$\frac{\partial \epsilon}{\partial t}+\frac{u_j}{H_j}\frac{\partial \epsilon}{\partial\xi_j}=\frac{1}{H_j}\frac{\partial}{\partial\xi_j}\Big(\frac{\Gamma_\epsilon}{H_j}\frac{\partial \epsilon}{\partial\xi_j}\Big)+\frac{\epsilon}{k}\cdot(C_1\cdot P_k-C_2\cdot\epsilon), \tag{2.2b}$$

where u_1, u_2 and u_3 are u, v and w respectively. Γ_k and Γ_ϵ are the diffusion coefficients defined as

$$\Gamma_k=v+v_t/\sigma_k \quad\text{and}\quad \Gamma_\epsilon=v+v_t/\sigma_\epsilon.$$

The production of turbulence P_k is given by

$$P_k=\frac{\tau_{11}}{H_1}\frac{\partial u}{\partial\xi}+\frac{\tau_{22}}{H_2}\frac{\partial v}{\partial\eta}+\frac{\tau_{33}}{H_3}\frac{\partial w}{\partial\zeta}+\tau_{12}\Big(\frac{1}{H_2}\frac{\partial u}{\partial\eta}+\frac{1}{H_1}\frac{\partial v}{\partial\xi}\Big)$$
$$+\tau_{13}\Big(\frac{1}{H_1}\frac{\partial w}{\partial\xi}+\frac{1}{H_3}\frac{\partial u}{\partial\zeta}\Big)+\tau_{23}\Big(\frac{1}{H_3}\frac{\partial v}{\partial\zeta}+\frac{1}{H_2}\frac{\partial w}{\partial\eta}\Big).$$

The typical constants of k-ϵ equations are used with C_μ=0.09, C_1=1.44, C_2=1.92, σ_k=1.0, and σ_ϵ=1.3.

In principle, there are four types of boundary conditions in hydrodynamic calculations.

1) **Fluid entry**

Along the fluid entry boundary, the convective flux is specified with measurements and the gradient of pressure is zero. The turbulent kinetic energy k and the dissipation rate ϵ are given by the empirical formulae:

$$k=0.00375(u^2+v^2+w^2),\quad \epsilon=\frac{u_*^3}{\kappa_1\zeta_p},$$

https://doi.org/10.4208/aamm.2014.m605 Published online by Cambridge University Press

where u_* =the bed shear velocity; ζ_p =the normal distance from the river bed to the nearest node; and von Karman constant $\kappa_1 = 0.41$.

2) **Fluid exit**

At the fluid exit boundary, zero velocity gradients are applied, and the pressure is specified with measurements. Zero gradient conditions are also used for the turbulent kinetic energy k, and the dissipation rate ϵ.

3) **Walls and river bed**

At the solid boundary, non-slip conditions are used so that all velocity-components set to zero, and a zero pressure gradient is also specified. Rather than non-slip conditions, the values of wall shear stress are more important for the fully developed turbulent flow. The wall-function method is used to calculate wall shear stress and bridges the fully developed turbulent region calculated by k-ϵ model and the solid boundary. The details of implementing wall-function method are presented in [17].

4) **Free surface**

The velocity-component normal to the free surface w is set to zero, and the pressure to the atmospheric value (or a zero gradient). The horizontal velocity-components u, v and the turbulent kinetic energy k are set to zero gradient conditions. The dissipation rate ϵ is given by

$$\epsilon = \frac{u_*^3}{\kappa_1}\left(\frac{1}{0.07h} + \frac{1}{\eta_{\min}}\right),$$

where h=the normal distance from the free surface to the river bed, and $\eta_{\min}$ =the minimum horizontal distance from the bank.

3 Numerical methods

3.1 Compact schemes

A high-order numerical method of three-dimensional hydrodynamic model is presented in this section. Compact schemes are employed for high-order spatial discretization. A sixth-order symmetric compact scheme [10, 18] is used to approximate the first order derivatives.

$$f'_{i-1} + 3f'_i + f'_{i+1} = \frac{7}{3h}(f_{i+1} - f_{i-1}) + \frac{1}{12h}(f_{i+2} - f_{i-2}). \tag{3.1}$$

Here, on a uniform computational mesh there is an equal node spacing $h = x_i - x_{i-1}$; and f' is the first order derivative of function $f(x)$, where subscript $1 < i < N$ is the node index. f'_i $(i = 1, \cdots, N)$ are solved together as a tridiagonal matrix.

A fifth-order upwind compact scheme [15, 18] is used to approximate the convection

https://doi.org/10.4208/aamm.2014.m605 Published online by Cambridge University Press

terms. Take the general convection term $C\cdot\partial f/\partial x$ for example to illustrate:

$$2f'_{i-1}+3f'_i=\frac{-3f_{i-2}-44f_{i-1}+36f_i+12f_{i+1}-f_{i+2}}{12h} \quad \text{for } C_i>0, \tag{3.2a}$$

$$2f'_{i+1}+3f'_i=\frac{-3f_{i+2}-44f_{i+1}+36f_i+12f_{i-1}-f_{i-2}}{12h} \quad \text{for } C_i<0. \tag{3.2b}$$

If C_i is postiove, a backward difference scheme (3.2a) is used for the spatial discretization, otherwise a forward difference scheme (3.2b) is used. Here C can be convection velocities u, v and w, and $\partial f/\partial x$ can be derivatives $\partial u_i/\partial\xi_j$ $(i=1,2,3;\ j=1,2,3)$.

Non-symmetry or small stencil boundary formulae are required at the nodes close to boundary. Hence, third-order boundary formulae (at nodes $i=1$ and $i=N$) and fourth-order near-boundary formulae (at nodes $i=2$ and $i=N-1$) are used [18].

$$i=1,\quad f'_1+2f'_2=\frac{-5f_1+4f_2+f_3}{2h},$$

$$i=2,\quad f'_1+4f'_2+f'_3=\frac{-3f_1+3f_3}{h}.$$

There are similar formulae at nodes $i=N$ and $i=N-1$.

3.2 Time-stepping procedure

The Reynolds-averaged fluid motion equations are calculated in two steps: 1) Integrate the momentum equations to obtain u^{n+1}, v^{n+1} and w^{n+1}; 2) Then, iterate the pressure equation to obtain p^{n+1}.

3.2.1 Integration of momentum equations

Integration of momentum equations is implemented with a four-stage modified Runge-Kutta scheme.

$$\boldsymbol{V}^{(1)}=\boldsymbol{V}^n, \tag{3.3a}$$

$$\boldsymbol{V}^{(2)}=\boldsymbol{V}^n+\frac{\Delta t}{4}\cdot\left(\frac{\partial \boldsymbol{V}}{\partial t}\right)^{(1)}, \tag{3.3b}$$

$$\boldsymbol{V}^{(3)}=\boldsymbol{V}^n+\frac{\Delta t}{3}\cdot\left(\frac{\partial \boldsymbol{V}}{\partial t}\right)^{(2)}, \tag{3.3c}$$

$$\boldsymbol{V}^{(4)}=\boldsymbol{V}^n+\frac{\Delta t}{2}\cdot\left(\frac{\partial \boldsymbol{V}}{\partial t}\right)^{(3)}, \tag{3.3d}$$

$$\boldsymbol{V}^{n+1}=\boldsymbol{V}^n+\Delta t\cdot\left(\frac{\partial \boldsymbol{V}}{\partial t}\right)^{(4)}, \tag{3.3e}$$

in which

$$\boldsymbol{V}=(u,v,w) \quad \text{and} \quad \frac{\partial \boldsymbol{V}}{\partial t}=\left(\frac{\partial u}{\partial t},\frac{\partial v}{\partial t},\frac{\partial w}{\partial t}\right),$$

https://doi.org/10.4208/aamm.2014.m605 Published online by Cambridge University Press

where the superscript index n is time level, and the superscripts (1), (2), (3) and (4) represent the sub-steps of Runge-Kutta scheme. To discretize the momentum equations, we rewrite (2.1b) this way.

$$\begin{aligned}\frac{\partial u}{\partial t}=&\frac{1}{H_1H_2H_3}\Big(\frac{\partial\tau_{11}H_2H_3}{\partial\xi}+\frac{\partial\tau_{12}H_1H_3}{\partial\eta}+\frac{\partial\tau_{13}H_1H_2}{\partial\zeta}\Big)+\frac{1}{H_1H_2}\Big(\tau_{12}\frac{\partial H_1}{\partial\eta}-\tau_{22}\frac{\partial H_2}{\partial\xi}\Big)\\&+\frac{1}{H_1H_3}\Big(\tau_{13}\frac{\partial H_1}{\partial\zeta}-\tau_{33}\frac{\partial H_3}{\partial\xi}\Big)-\Big[\frac{u}{H_1}\frac{\partial u}{\partial\xi}+\frac{v}{H_2}\frac{\partial u}{\partial\eta}+\frac{w}{H_3}\frac{\partial u}{\partial\zeta}\Big]\\&-\Big[\frac{v}{H_1H_2}\Big(u\frac{\partial H_1}{\partial\eta}-v\frac{\partial H_2}{\partial\xi}\Big)+\frac{w}{H_1H_3}\Big(u\frac{\partial H_1}{\partial\zeta}-w\frac{\partial H_3}{\partial\xi}\Big)+\frac{1}{H_1}\frac{\partial p}{\partial\xi}\Big].\end{aligned}\tag{3.4}$$

The derivatives on the right hand side are discretized by the symmetric compact scheme except the convection terms

$$\Big(\frac{u}{H_1}\frac{\partial u}{\partial\xi},\quad \frac{v}{H_2}\frac{\partial u}{\partial\eta}\quad\text{and}\quad \frac{w}{H_3}\frac{\partial u}{\partial\zeta}\Big)$$

discretized by the upwind compact scheme. Then substitute the value to the Runge-Kutta scheme to obtain u^{n+1}. The stresses τ_{ij} are fully discretized by the symmetric compact scheme and computed before the semi-discrete momentum equation calculation. We obtained v^{n+1} and w^{n+1} with the similar procedure by (2.1c) and (2.1d).

3.2.2 Iteration of pressure equation

A pressure equation is proposed to compute p^{n+1}, which is derived from the momentum and continuity equations [19], and written as

$$\begin{aligned}&\frac{\partial}{\partial\xi}\Big(\frac{H_2H_3}{H_1}\frac{\partial p}{\partial\xi}\Big)+\frac{\partial}{\partial\eta}\Big(\frac{H_1H_3}{H_2}\frac{\partial p}{\partial\eta}\Big)+\frac{\partial}{\partial\zeta}\Big(\frac{H_1H_2}{H_3}\frac{\partial p}{\partial\zeta}\Big)\\=&\frac{\partial H_2H_3\Phi_1}{\partial\xi}+\frac{\partial H_1H_3\Phi_2}{\partial\eta}+\frac{\partial H_1H_2\Phi_3}{\partial\zeta}+\frac{1}{\Delta t}\Big(\frac{\partial H_2H_3u}{\partial\xi}+\frac{\partial H_1H_3v}{\partial\eta}+\frac{\partial H_1H_2w}{\partial\zeta}\Big),\end{aligned}\tag{3.5}$$

in which

$$\begin{aligned}\Phi_1=&\frac{1}{H_1H_2H_3}\Big(\frac{\partial\tau_{11}H_2H_3}{\partial\xi}+\frac{\partial\tau_{12}H_1H_3}{\partial\eta}+\frac{\partial\tau_{13}H_1H_2}{\partial\zeta}\Big)+\frac{1}{H_1H_2}\Big(\tau_{12}\frac{\partial H_1}{\partial\eta}-\tau_{22}\frac{\partial H_2}{\partial\xi}\Big)\\&+\frac{1}{H_1H_3}\Big(\tau_{13}\frac{\partial H_1}{\partial\zeta}-\tau_{33}\frac{\partial H_3}{\partial\xi}\Big)-\Big[\frac{u}{H_1}\frac{\partial u}{\partial\xi}+\frac{v}{H_2}\frac{\partial u}{\partial\eta}+\frac{w}{H_3}\frac{\partial u}{\partial\zeta}\Big]\\&-\Big[\frac{v}{H_1H_2}\Big(u\frac{\partial H_1}{\partial\eta}-v\frac{\partial H_2}{\partial\xi}\Big)+\frac{w}{H_1H_3}\Big(u\frac{\partial H_1}{\partial\zeta}-w\frac{\partial H_3}{\partial\xi}\Big)\Big],\end{aligned}\tag{3.6a}$$

https://doi.org/10.4208/aamm.2014.m605 Published online by Cambridge University Press

$$\Phi_2=\frac{1}{H_1H_2H_3}\Big(\frac{\partial\tau_{12}H_2H_3}{\partial\xi}+\frac{\partial\tau_{22}H_1H_3}{\partial\eta}+\frac{\partial\tau_{23}H_1H_2}{\partial\zeta}\Big)+\frac{1}{H_1H_2}\Big(\tau_{12}\frac{\partial H_2}{\partial\xi}-\tau_{11}\frac{\partial H_1}{\partial\eta}\Big)$$
$$+\frac{1}{H_2H_3}\Big(\tau_{23}\frac{\partial H_2}{\partial\zeta}-\tau_{33}\frac{\partial H_3}{\partial\eta}\Big)-\Big[\frac{u}{H_1}\frac{\partial v}{\partial\xi}+\frac{v}{H_2}\frac{\partial v}{\partial\eta}+\frac{w}{H_3}\frac{\partial v}{\partial\zeta}\Big]$$
$$-\Big[\frac{w}{H_2H_3}\Big(v\frac{\partial H_2}{\partial\zeta}-w\frac{\partial H_3}{\partial\eta}\Big)+\frac{u}{H_1H_2}\Big(v\frac{\partial H_2}{\partial\xi}-u\frac{\partial H_1}{\partial\eta}\Big)\Big], \tag{3.6b}$$

$$\Phi_3=\frac{1}{H_1H_2H_3}\Big(\frac{\partial\tau_{13}H_2H_3}{\partial\xi}+\frac{\partial\tau_{23}H_1H_3}{\partial\eta}+\frac{\partial\tau_{33}H_1H_2}{\partial\zeta}\Big)+\frac{1}{H_1H_3}\Big(\tau_{13}\frac{\partial H_3}{\partial\xi}-\tau_{11}\frac{\partial H_1}{\partial\zeta}\Big)$$
$$+\frac{1}{H_2H_3}\Big(\tau_{23}\frac{\partial H_3}{\partial\eta}-\tau_{22}\frac{\partial H_2}{\partial\zeta}\Big)-\Big[\frac{u}{H_1}\frac{\partial w}{\partial\xi}+\frac{v}{H_2}\frac{\partial w}{\partial\eta}+\frac{w}{H_3}\frac{\partial w}{\partial\zeta}\Big]$$
$$-\Big[\frac{u}{H_1H_3}\Big(w\frac{\partial H_3}{\partial\xi}-u\frac{\partial H_1}{\partial\zeta}\Big)+\frac{v}{H_2H_3}\Big(w\frac{\partial H_3}{\partial\eta}-v\frac{\partial H_3}{\partial\zeta}\Big)\Big]. \tag{3.6c}$$

The derivatives on the right hand side of (3.6a)-(3.6c) are discretized by the compact schemes in the similar way to the semi-discrete momentum equations. In the mean time, the derivatives of p on the left hand side of (3.5) are discretized by the central difference scheme constructed on half-node grids

$$\frac{\big(\frac{H_2H_3}{H_1}\big)_{i+\frac{1}{2},j,k}p_{i+1,j,k}-2\big(\frac{H_2H_3}{H_1}\big)_{i,j,k}p_{i,j,k}+\big(\frac{H_2H_3}{H_1}\big)_{i-\frac{1}{2},j,k}p_{i-1,j,k}}{(\Delta\xi)^2}$$
$$\frac{\big(\frac{H_1H_3}{H_2}\big)_{i,j+\frac{1}{2},k}p_{i,j+1,k}-2\big(\frac{H_1H_3}{H_2}\big)_{i,j,k}p_{i,j,k}+\big(\frac{H_1H_3}{H_2}\big)_{i,j-\frac{1}{2},k}p_{i,j-1,k}}{(\Delta\eta)^2}$$
$$\frac{\big(\frac{H_1H_2}{H_3}\big)_{i,j,k+\frac{1}{2}}p_{i,j,k+1}-2\big(\frac{H_1H_2}{H_3}\big)_{i,j,k}p_{i,j,k}+\big(\frac{H_1H_2}{H_3}\big)_{i,j,k-\frac{1}{2}}p_{i,j,k-1}}{(\Delta\zeta)^2}$$
$$=\frac{\partial H_2H_3\Phi_1^{n+1}}{\partial\xi}+\frac{\partial H_1H_3\Phi_2^{n+1}}{\partial\eta}+\frac{\partial H_1H_2\Phi_3^{n+1}}{\partial\zeta}+\frac{\big(\frac{\partial H_2H_3u}{\partial\xi}+\frac{\partial H_1H_3v}{\partial\eta}+\frac{\partial H_1H_2w}{\partial\zeta}\big)^{n+1}}{\Delta t}. \tag{3.7}$$

Here, the values at the half-node grids are two-point averages over the nearest nodes. We can obtain p^{n+1} by solving the Eq. (3.7). The initial value is imposed to p^n for accelerating the convergence.

The k-ϵ equations are solved in a similar way to the momentum equations. The flow field computation is carried out until a specified criterion is met.

4 The water level equation

The water level of a natural river or a open channel is a routine computation quantity of hydrodynamic simulation. Following the work of Wu et al. [4], a water level equation in an orthogonal curvilinear coordinate is derived in this section. The two-dimensional

https://doi.org/10.4208/aamm.2014.m605 Published online by Cambridge University Press

depth-average momentum-equations for a shallow open channel flow are obtained by vertical integration of momentum equations (2.1b) and (2.1c)

$$\frac{\partial \bar{u}}{\partial t}+\frac{\bar{u}}{H_1}\frac{\partial \bar{u}}{\partial \xi}+\frac{\bar{v}}{H_2}\frac{\partial \bar{u}}{\partial \eta}+\frac{\bar{v}}{H_1H_2}\left(\bar{u}\frac{\partial H_1}{\partial \eta}-\bar{v}\frac{\partial H_2}{\partial \xi}\right)+\frac{g}{H_1}\frac{\partial h}{\partial \xi}+gm^2\bar{u}\frac{\sqrt{\bar{u}^2+\bar{v}^2}}{h^{\frac{4}{3}}}$$
$$=\frac{1}{H_1H_2}\left(\frac{\partial \bar{\tau}_{11}H_2}{\partial \xi}+\frac{\partial \bar{\tau}_{12}H_1}{\partial \eta}+\bar{\tau}_{12}\frac{\partial H_1}{\partial \eta}-\bar{\tau}_{22}\frac{\partial H_2}{\partial \xi}\right), \tag{4.1a}$$

$$\frac{\partial \bar{v}}{\partial t}+\frac{\bar{u}}{H_1}\frac{\partial \bar{v}}{\partial \xi}+\frac{\bar{v}}{H_2}\frac{\partial \bar{v}}{\partial \eta}+\frac{\bar{u}}{H_1H_2}\left(\bar{v}\frac{\partial H_2}{\partial \xi}-\bar{u}\frac{\partial H_1}{\partial \eta}\right)+\frac{g}{H_2}\frac{\partial h}{\partial \eta}+gm^2\bar{v}\frac{\sqrt{\bar{u}^2+\bar{v}^2}}{h^{\frac{4}{3}}}$$
$$=\frac{1}{H_1H_2}\left(\frac{\partial \bar{\tau}_{12}H_2}{\partial \xi}+\frac{\partial \bar{\tau}_{22}H_1}{\partial \eta}+\bar{\tau}_{12}\frac{\partial H_2}{\partial \xi}-\bar{\tau}_{11}\frac{\partial H_1}{\partial \eta}\right), \tag{4.1b}$$

where h =the water level; $\bar{u}$ and $\bar{v}$ =the depth-average velocity in the ξ and η directions respectively; $\bar{\tau}_{11}$, $\bar{\tau}_{12}$ and $\bar{\tau}_{22}$ =the depth-average turbulent stresses; and m =Manning coefficient. Then a water level equation is derived from the depth-average momentum-equations by partial differentiating ξ-component momentum-equation (4.1a) with respect to ξ and η-component momentum-equation (4.1b) with respect to η, as follows:

$$\frac{\partial}{\partial \xi}\left(\frac{H_2}{H_1}\frac{\partial h}{\partial \xi}\right)+\frac{\partial}{\partial \eta}\left(\frac{H_1}{H_2}\frac{\partial h}{\partial \eta}\right)=\frac{Q}{g}, \tag{4.2}$$

in which

$$\begin{aligned}Q=&\frac{\partial H_2}{\partial \xi}\left\{\frac{1}{H_1H_2}\left(\frac{\partial \bar{\tau}_{11}H_2}{\partial \xi}+\frac{\partial \bar{\tau}_{12}H_1}{\partial \eta}+\bar{\tau}_{12}\frac{\partial H_1}{\partial \eta}-\bar{\tau}_{22}\frac{\partial H_2}{\partial \xi}\right)\right.\\&\left.-\left[\frac{\bar{u}}{H_1}\frac{\partial \bar{u}}{\partial \xi}+\frac{\bar{v}}{H_2}\frac{\partial \bar{u}}{\partial \eta}+\frac{\bar{v}}{H_1H_2}\left(\bar{u}\frac{\partial H_1}{\partial \eta}-\bar{v}\frac{\partial H_2}{\partial \xi}\right)+gm^2\bar{u}\frac{\sqrt{\bar{u}^2+\bar{v}^2}}{h^{\frac{4}{3}}}\right]\right\}\\&+\frac{\partial H_1}{\partial \eta}\left\{\frac{1}{H_1H_2}\left(\frac{\partial \bar{\tau}_{12}H_2}{\partial \xi}+\frac{\partial \bar{\tau}_{22}H_1}{\partial \eta}+\bar{\tau}_{12}\frac{\partial H_2}{\partial \xi}-\bar{\tau}_{11}\frac{\partial H_1}{\partial \eta}\right)\right.\\&\left.-\left[\frac{\bar{u}}{H_1}\frac{\partial \bar{v}}{\partial \xi}+\frac{\bar{v}}{H_2}\frac{\partial \bar{v}}{\partial \eta}+\frac{\bar{u}}{H_1H_2}\left(\bar{v}\frac{\partial H_2}{\partial \xi}-\bar{u}\frac{\partial H_1}{\partial \eta}\right)+gm^2\bar{v}\frac{\sqrt{\bar{u}^2+\bar{v}^2}}{h^{\frac{4}{3}}}\right]\right\}.\end{aligned}$$

The discretization of the water level equation is similar to the treatment of pressure equation. The derivatives on the right hand side are discretized by compact schemes, while the derivatives of the water level h on the left hand side are discretized by the central difference scheme. The water level calculation may be restricted to flow with gradual variation [4].

4.1 Calculation sequence

The three-dimensional hydrodynamic model is solved as follows:

1. Generate the computational mesh.

https://doi.org/10.4208/aamm.2014.m605 Published online by Cambridge University Press

2. Start from an initial flow field including turbulence quantities.
3. Solve the momentum equations to obtain the flow field u^{n+1}, v^{n+1} and w^{n+1}.
4. Solve the pressure equation to obtain the pressure field p^{n+1}.
5. Solve the k- and ϵ-equations to obtain k^{n+1} and ϵ^{n+1} and update the eddy viscosity v_t.
6. Solve the water level equation to obtain the water level h^{n+1} and adjust the mesh.
7. Return to step 3 and repeat the calculation proceed until a specified criterion is met or a specified time is covered.

5 Numerical validation of present solver

In this section, a typical 180° curved open channel flow is simulated by the present method and SIMPLEC algorithm. The computed results are compared with measured data to validate the present method.

According to [16], a 180° curved flume of the dimension is constructed with

$$R_i = 3.4\text{m}; \quad R_o = 5.1\text{m}; \quad L = 6\text{m},$$

where R_i =the inside diameter; R_o =the outside diameter; and L =the length of the straight segments. According to the experimental data, the entry quantity $Q_{in} = 0.19\text{m}^3/\text{s}$; the downstream water level $h_{out} = 0.18\text{m}$; Manning coefficient $m = 0.012$; and the molecular viscosity of water $v = 1.0 \times 10^{-6}\text{m}^2/\text{s}$. There are $101 \times 41 \times 13$ grid nodes in the streamwise, lateral and vertical directions respectively. The temporal step is set to $\Delta t = 0.001\text{s}$. The specified criterion for both methods to stop the computation is

$$\frac{\Delta V}{\Delta t} < 10^{-2},$$

in which

$$\Delta V = \max\left(\sqrt{(u^{n+1}-u^n)^2+(v^{n+1}-v^n)^2+(w^{n+1}-w^n)^2}\right) < 10^{-5}.$$

The measured and computed distributions of the depth-average ξ-component velocity u at various cross-sections are shown in Fig. 1. Here, B =the width of the cross-section, and η/B =the non-dimensional distance from the inner bank. In the section 0° and 30°, the depth-average velocity distributions computed by the compact scheme (solid line) and SIMPLEC algorithm (dashed line) agree well with the measured data (filled square). Then, the maximum of depth-average velocity shift from the inner bank (section 0° and 30°) to the outer bank (section 60°, 90°, 120° and 180°) in the bend. From section 60° to 180°, the depth-average velocity distributions computed by the compact scheme approximate to the measured data better than those from SIMPLEC algorithm. The maximum

https://doi.org/10.4208/aamm.2014.m605 Published online by Cambridge University Press

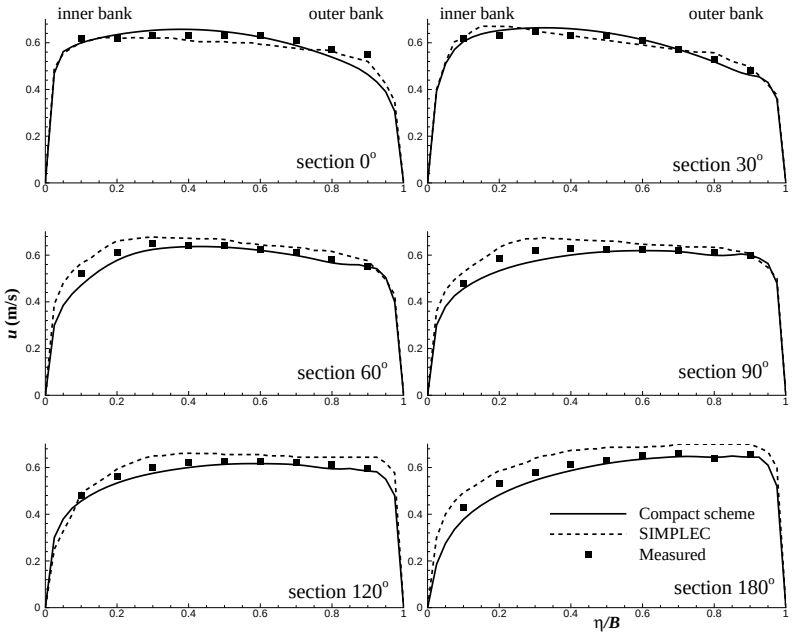


Figure 1: Depth-averaged velocity distributions at cross-sections.

relative error of the compact scheme method is 3.3%, which is much less than 9.4% from SIMPLEC algorithm. The relative error is defined as

$$\text{Relative Error} = \frac{\text{Computed Value-Measured Value}}{\text{Measured Value}}.$$

The results indicate that the compact scheme method can accurately predict the velocities and has better accuracy than SIMPLEC algorithm in a curved shallow open channel computation. Furthermore, the method represents smoother depth-average velocity profiles at cross-sections.

The measured and computed streamwise distributions of water level are shown in Fig. 2. Here, S =the distance to the entrance; L =the length of the flume centre line; S/L =the non-dimension distance to the entrance; and the non-dimensional water level $H=(h-h_{out})/h_{out}$. At $B/8$ from the inner bank (the lower branch of water level line), the results from the compact scheme approximate closely to the measured data, whereas those from SIMPLEC algorithm doesn't approximate well. At $B/8$ from the outer bank (The higher branch of water level line), the results from the compact scheme are close to the measured data in the straight segments and the middle of curved flume, while those from SIMPLEC algorithm only agree in part with the segment of curved flume. At the centre line, although results of both methods do not match the measured data well, the results from the compact scheme are closer to the measured data. The relative errors in the water level computed by the compact scheme method are given in Table 1. The

https://doi.org/10.4208/aamm.2014.m605 Published online by Cambridge University Press

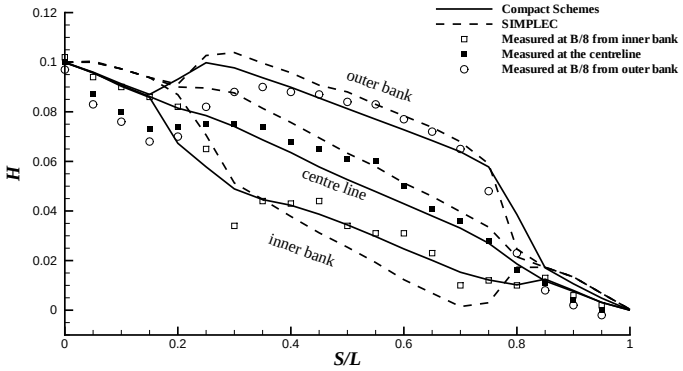


Figure 2: Computed and measured water level along the flume.

relative errors are on the order of 10^{-3}, which meets the needs of most hydraulic applications. The water level equation can predict the water level in a curved open channel with good accuracy.

Comparisons on different grid number meshes can show how the accuracy of the present method depends on the grid sizes. We made the comparisons with the same CFL number on account of the numerical accuracy depending on the CFL number. It is found that the finer meshes improve the numerical accuracy. The accuracy is improved roughly 3% with 1.5-times number grids and roughly 5% with double number grids.

Table 1: Relative errors in the water level computed by the compact scheme method.

S/L	0.1	0.2	0.3	0.4	0.5	0.6	0.7	0.8	0.9	Average
inner bank	0.0003	0.0147	0.0149	0.0007	0.0004	0.0063	0.0053	0.0002	0.0020	0.0050
centre line	0.0108	0.0075	0.0009	0.0044	0.0084	0.0071	0.0029	0.0027	0.0036	0.0054
outer bank	0.0153	0.0231	0.0097	0.0019	0.0027	0.0043	0.0011	0.0156	0.0086	0.0091

6 Simulation of flow in a natural river

In this section, flow in a natural river with continuous bends and sloped banks is simulated by the new method. The Guanxi River is 7200m long and 30m wide at the bed with a trapezoidal cross-section and 1:2 sloped. The mean bed elevation is 4m, and Manning coefficient $m=0.025$ according to the measured data. The first bend is 3729.58m long with a radius of 2514.50m, and the second bend is 3444.72m long with a radius of 4352.12m. There are $721\times21\times11$ grids in the streamwise, lateral and vertical directions respectively.

The entry quantity $Q_{in}=30.0\text{m}^3/\text{s}$, which is estimated with annual mean values measured in the hydrological station 1; And the downstream water level $h_{out}=9\text{m}$, which is estimated with the annual mean values measured in the hydrological station 3 and corrected with the measured data in the hydrological station 2. Besides, there are lat-

https://doi.org/10.4208/aamm.2014.m605 Published online by Cambridge University Press

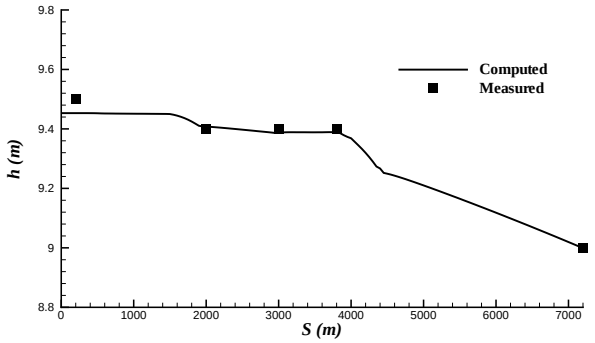


Figure 3: Computed and measured water level along the centre line in the Guanxi River.

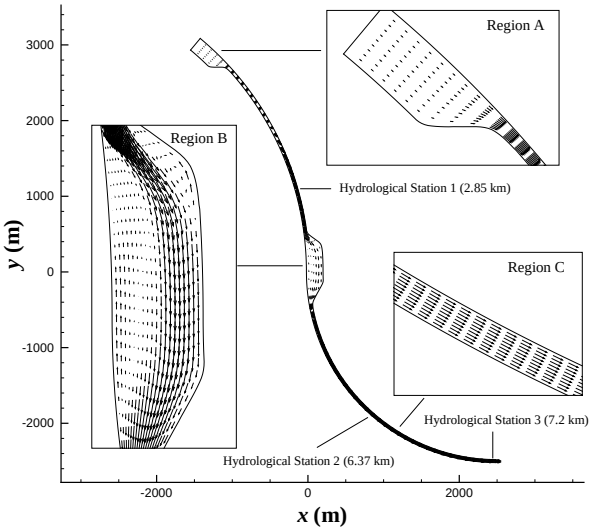


Figure 4: Distributions of velocity vector in the Guanxi River at 7m altitude plane.

eral entry quantities $q_i = 24.0\text{m}^3/\text{s}$ on the bank. Other boundary conditions have been described in Section 2.

The streamwise distributions of computed and measured water level in the centre line of Guanxi River are shown in Fig. 3. The computed water level generally agrees with the measured data.

The distributions of velocity vector at 7m altitude horizontal plane of the Guanxi River are shown in Fig. 4. The new method performs a high resolution pattern of flow in the Guanxi River. In the broad entry region A, the stream is under low-speed situation. The river narrows at 400m downstream. Then a 2600m long channel is presented with high-speed flow motion. Coming into the middle of the Guanxi River, there is a 1000m long broad region B. Two counter-rotating horizontal circulations appear here which are

https://doi.org/10.4208/aamm.2014.m605 Published online by Cambridge University Press

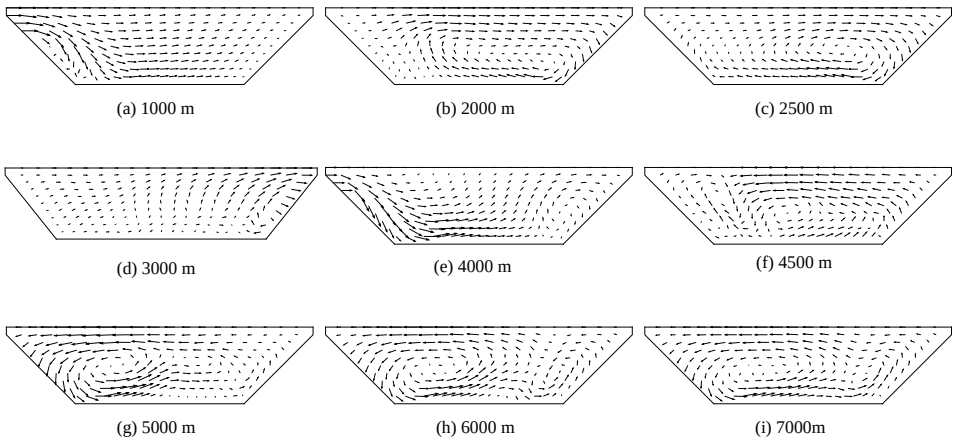


Figure 5: Distributions of secondary velocity vector at cross-sections.

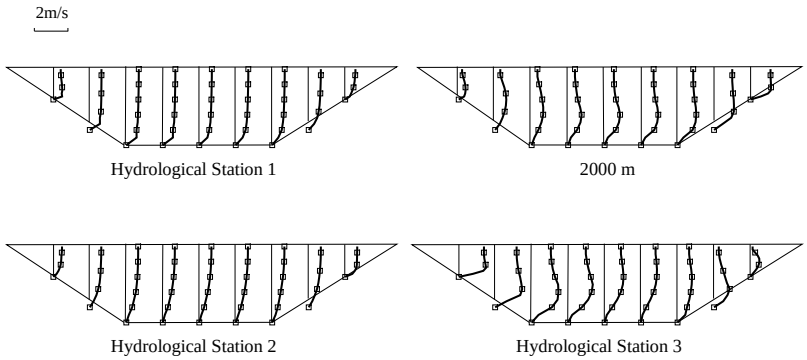


Figure 6: Comparison of main flow velocity at cross-sections.

separated by the high-speed stream in the lateral of the centre line. The minor circulation on the right of the channel is anti-clockwise, whereas the major circulation on the left is clockwise. At last, a 3200m long river segment C associates the Guanxi River with the Gucheng Lake, where the distribution of velocity vector is uniform.

The distributions of velocity vector at cross-sections are shown in Fig. 5. The secondary current is clockwise if bend turns to left (Fig. 5(c)) and anti-clockwise if bend turns to right (Fig. 5(h)) due to the centrifugal force effect. Secondary currents turn to be stronger in the presence of lateral entry quantities on the bank (Figs. 5(a) and (e)). The longitudinal vortexes develop downstream and influence the currents there(Figs. 5(b), (f) and (g)).

Computed and measured distributions of main flow velocity at various cross-sections are shown in Fig. 6. There are good agreements between computed (solid lines) and measured data (hallow squares). The new method is validated to be an accurate and reliable approach to study three-dimensional hydrodynamics with complex flow by simulating the Guanxi River.

https://doi.org/10.4208/aamm.2014.m605 Published online by Cambridge University Press

7 Conclusions

In this study, a new numerical method is developed to solve the three-dimensional Reynolds-averaged Navier-Stokes equations with the k-ϵ turbulence model. A two-dimensional equation is derived from the depth-averaged momentum equations to predict the water level.

Flow in a 180° curved laboratory flume is computed to validate the proposed method. The results from the compact scheme show better accuracy than those from SIMPLEC algorithm by comparing the distributions of the computed and measured velocities at different cross-sections. The small relative errors in water levels show that the water level equation can accurately predict the water level. Then the method is applied to study three-dimensional hydrodynamics in a natural river with continuous bends and sloped banks. The simulated results are in accordance with the measured data. Three-dimensional flow features such as horizontal circulations and secondary currents are displayed with fine resolution and conform to the observations.

In conclusions, this high-order method is an efficient approach to solve three-dimensional hydrodynamic equations and also an accurate tool to study three-dimensional hydrodynamics in a natural river.

Acknowledgments

This work is supported by the National Natural Science Foundation of China (Grant No. 11172143) and Research Innovation Program for College Graduates of Jiangsu Province (CXZZ13 0518).

References

[1] A. N. Papanicolaou, M. Elhakeem and G. Krallis et al., *Sediment transport modeling review-current and future developments,* J. Hydraul. Eng., 134 (2008), pp. 1–14.
[2] A. O. Demuren and W. Rodi, *Calculation of flow and pollutant dispersion in meandering channels,* J. Fluid. Mech., 172 (1986), pp. 63–92.
[3] J. Ye and J. A. McCorquodale, *Simulation of curved open channel flows by 3D hydrodynamic model,* J. Hydraul. Eng., 124 (1998), pp. 687–698.
[4] W. Wu, W. Rodi and T. Wenka, *3D numerical modeling of flow and sediment transport in open channels,* J. Hydraul. Eng., 126 (2000), pp. 4–15.
[5] N. Rüther and N. R. Olsen, *Three-dimensional modeling of sediment transport in a narrow* 90° *channel bend,* J. Hydraul. Eng., 131 (2005), pp. 917–920.
[6] M. L. Zhang and Y. M. Shen, *Application of 3-D RNG k-ϵ turbulence model of meandering river,* J. Hydroelec. Eng., 26 (2007), pp. 86–91 (in Chinese).
[7] A. Khosronejad, C. D. Rennie and S. A. A. Salehi Neyshabouri et al., *3D numerical modeling of flow and sediment transport in laboratory channel bends,* J. Hydraul. Eng., 133 (2007), pp. 1123–1134.

https://doi.org/10.4208/aamm.2014.m605 Published online by Cambridge University Press

[8] R. FEURICH AND N. R. B. OLSEN, *Three-dimensional modeling of nonuniform sediment transport in an S-shaped channel,* J. Hydraul. Eng., 137 (2011), pp.493-495.
[9] J. ZENG, G. CONSTANTINESCU AND L. WEBER, *A 3D non-hydrostatic model to predict flow and sediment transport in loose-bed channel bends,* J. Hydraul. Res., 46 (2008), pp. 356–372.
[10] S. K. LELE, *Compact finite difference schemes with spectral-like resolution,* J. Comput. Phys., 103 (1992), pp. 16–42.
[11] J. M. C. PEREIRA, M. H. KOBAYASHI AND J. C. F. PEREIRA, *A fourth-order-accurate finite volume compact method for the incompressible Navier-Stokes solutions,* J. Comput. Phys., 167 (2001), pp. 217–243.
[12] A. HOKPUNNA AND M. MANHART, *Compact fourth-order finite volume method for numerical solutions of Navier-Stokes equations on staggered grids,* J. Comput. Phys., 229 (2010), pp. 7545–7570.
[13] A. A. ELHAMI, H. S. KAZEMZADEH AND F. MASHAYEK, *Evaluation of a fourth-order finite-volume compact scheme for LES with explicit filtering,* Numer. Heat. Tr. B-Fund., 48 (2005), pp. 147–163.
[14] S. NAGARAJAN, S. K. LELE AND J. H. FERZIGER, *A robust high-order compact method for large eddy simulation,* J. Comput. Phys., 191 (2003), pp. 392–419.
[15] D. FU AND Y. MA, *A high order accurate difference scheme for complex flow fields,* J. Comput. Phys., 134 (1997), PP. 1–15.
[16] H. J. DE VRIEND, *A mathematical model of steady flow in curved shallow channels,* J. Hydraul. Res., 15 (1977), pp. 37–54.
[17] D. NOAT, *Response of channel flow to roughness heterogeneity*, J. Hydraul. Eng., 110 (1984), pp. 1568–1587.
[18] C. LU, W. CAO AND Y. ZHANG ET AL., *Large eddies induced by local impulse at wall of boundary layer with pressure gradients,* Prog. Nat. Sci., 18 (2008), pp. 873–878.
[19] F. H. HARLOW AND J. E. WELCH, *Numerical calculation of time-dependent viscous incompressible flow of fluid with free surface,* Phys. Fluids., 8 (1965), pp. 2182.

https://doi.org/10.4208/aamm.2014.m605 Published online by Cambridge University Press